DOI: 10.1002/ejic.200700936

Tunable Synthesis of Various Hierarchical Structures of $In(OH)_3$ and In_2O_3 Assembled by Nanocubes

Li-Yong Chen,[a] Yan-Ge Zhang,[b] Wei-Zhi Wang,[a] and Zu-De Zhang*[a]

Keywords: Indium / Crystal growth / Hydrothermal synthesis / Photoluminescence

We show a simple way to synthesize morphology-controllable $In(OH)_3$ nanostructures by utilizing an amine-assisted hydrolysis of In^{3+} cations under various reaction temperatures. By annealing as-prepared $In(OH)_3$ precursors at 400 °C in air, we obtained In_2O_3 nanocrystals that inherited the morphologies of their precursors while still slightly distorted due to the dehydration process of $In(OH)_3$. This dehydration process that transforms $In(OH)_3$ into In_2O_3 was studied by thermogravimetry and differential thermal analysis. X-ray powder diffraction, field emission scanning electron microscopy, transmission electron microscopy, and photoluminescence spectra were used to characterize the as-obtained products. Fourier transform infrared absorption spectra were recorded to investigate the effect of ethylenediamine in $In(OH)_3$. It was found that the amines play ternary roles, which include being the alkaline media, the coordinating agent, and the surface-anchored organic molecules.

Introduction

Nanomaterials have received considerable attention due to their potential applications in chemistry, physics, electronics, biotechnology, and materials science. Recently, hierarchical nanoarchitectures assembled from nanoscaled units were prepared and widely employed in many areas, as they provide potential for obtaining higher functionality and performance. For example, micro- or nanometer-scale hollow spheres with controllable structure, composition, and properties have shown to be promising in many fields such as catalysis, low-density structural materials, and capsules for the controlled release of medication and dyes.[1–4] Therefore, the synthesis of three-dimensional nano/microstructures with complex architectures has been an exciting area of investigation because of their great potential applications. Self-assembly of nanoscaled building blocks has attracted significant interest in materials synthesis and device fabrication.[5–24] Driving forces of self-organized aggregation include capillary effects,[19] surface tension,[20] electric[21] and magnetic[22] forces, chemical bonding,[23] hydrogen bonding,[10] and hydrophobic interactions.[24] Organic ligands combined with nanocrystals binding affinities can promote self-assembly, driven by the interactions between surface-adsorbed ligands instead of between the nanocrystals themselves. Hence, surface-stabilized nanocrystals acting as nanoscale building blocks can provide an alternate pathway for the spontaneous self-assembly of nanounits into various ordered nanostructures.

Indium oxide (In_2O_3) nanostructures, an important n-type semiconductor with a direct bandgap of 3.55–3.75 eV, hold great promise for applications in microelectronic areas and ultrasensitive gas sensors.[25–30] Previously, In_2O_3 materials were obtained by annealing their $In(OH)_3$ or InOOH precursors with the desired morphology, including In_2O_3 nanocubes,[31] nanofibers,[32] nanotubes,[33] hollow microspheres,[30] nanorod bundles and spheres,[34] porous nanostructures,[35] and different nanocrystals.[36] In situ release of water from oxyhydroxide materials during the decomposition process would retain the morphology of their precursors. In this work, we provide a facile approach for the tunable synthesis of $In(OH)_3$ through the assembly of nanocubes into different spherical micro- and nanostructures in aqueous solutions on a large scale. The synthetic route is interesting to study in order to understand the self-assembly of building blocks and helps to prepare other functional nanomaterials. The lattice planes of these assembled nanocubes are observed to be well aligned. Ethylenediamine (En) and reaction temperature play crucial roles in the aggregation of $In(OH)_3$ nanocubes from random structures to spherical structures. En molecules, as surface-anchored molecules, adsorb onto the lateral surfaces of $In(OH)_3$ nanocrystals and drive the aggregation growth of these nanocrystals by hydrogen bonding. Furthermore, the as-obtained In_2O_3 may well inherit the morphologies of $In(OH)_3$ by annealing its precursors at 400 °C under ambient pressure and in air.

[a] Department of Chemistry, University of Science and Technology of China,
Hefei, Anhui, 230026, P. R. China
Fax: +86-551-3601592
E-mail: zzd@ustc.edu.cn
[b] Institute of Surface Micro and Nano Materials, Xuchang University,
Xuchang, Henan, 461000, P. R. China

Results and Discussion

Structural and Morphological Characterization of Self-Assembled $In(OH)_3$ Nanocubes

$In(OH)_3$ nanocubes were synthesized by a hydrothermal process at 210 °C for 16 h with En as both the alkaline media and the coordinating agent. X-ray diffraction was used to verify the crystal structures and the phase purity of the samples. The typical XRD pattern (Figure 1) shows that all reflection peaks can be indexed to the body-centered cubic (*bcc*) phase of $In(OH)_3$ (JCPDS No.85–1338, a = 7.979 Å).

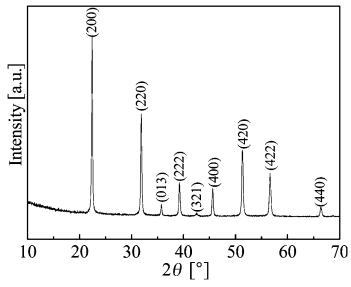

Figure 1. XRD pattern of $In(OH)_3$ prepared at 210 °C for 16 h.

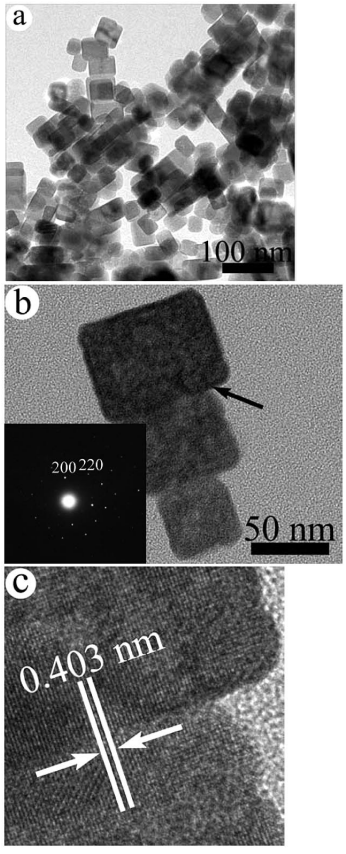

Figure 2. TEM image of $In(OH)_3$ nanocubes prepared at 210 °C for 16 h: (a) at low-magnification and (b) typical aggregation of nanocubes (the inset is its corresponding SAED pattern). HRTEM image (c) obtained from the areas marked with a black arrow as shown in (b).

No other impurities, such as InOOH or In_2O_3, were detected, which indicates the high purity of the sample. Other $In(OH)_3$ samples prepared in this work presented similar profiles.

The morphologies and structures of the obtained $In(OH)_3$ products were illustrated by transmission electron microscopy (TEM) images, HRTEM images, and SAED pattern (Figure 2). A typical TEM image of the as-obtained $In(OH)_3$ (Figure 2a) indicates that the sample possesses the morphology of regular nanocubes with a mean edge of 20–50 nm. Interestingly, all nanocubes are almost conglutinated (Figure 2a). Figure 2b shows a representative magnified TEM image of the nanocubes. Detailed observation suggests that each nanocube adheres to another nanocube as indicated by the black arrow. The inserted SAED pattern of these nanocubes is recorded with the electron beam along the [001] zone axis of the $In(OH)_3$ cubic phase. The diffraction spots can be indexed to (200) and (220) crystal planes. The corresponding HRTEM image (Figure 2c) of the coalescent area shows lattice fringe with spacing of ca. 0.403 nm, which is consistent with the (020) crystal plane of $In(OH)_3$. It can be seen that the (020) lattice planes of the depicted nanocubes are well aligned. Both the SAED pattern and the HRTEM image reveal that these aggregated nanocubes are single-crystalline in nature and confirm the well-oriented aggregation of the crystal planes along the [010] direction.

Mechanism of Formation

Although the exact mechanism of formation for the self-assembly of the $In(OH)_3$ nanocubes is still not clear, the binding affinity of the organic molecules at the interfaces of the nanocubes is undoubtedly significant. The binding affinity so strong that the nanocrystals are highly stabilized, which prevents further crystal growth from occurring within the aggregates. In this case, the nanocrystals can become ordered by organic interactions at the interfaces between the hybrid building blocks.[37]

In the present systems, it was found that En is indispensable for the self-assembly of the nanocubes. On the basis of the results of others,[38,39] many metallic elements or cations can coordinate with En molecules to form fairly stable complexes. Here, En acts as a coordinating agent and also provides an alkaline media for the In^{3+} cations, which facilitates the hydrolysis of In^{3+} to form $In(OH)_3$ nanocubes. The surface of $In(OH)_3$ may chemically adsorb En molecules by hydrogen bonding between the N–H group of En and the O–H group of $In(OH)_3$. This is confirmed by our FTIR investigation (Figure 3a). Thus, En also serves as an anchored organic molecule, which favors the oriented aggregation of nanocubes. The whole process can be expressed as follows:[40]

$$In^{3+} + 2\ En \rightarrow [In(En)_2]^{3+}$$

$$[In(En)_2]^{3+} + 3\ OH^- \rightarrow In(OH)_3(En)_m + (2 - m)\ En$$

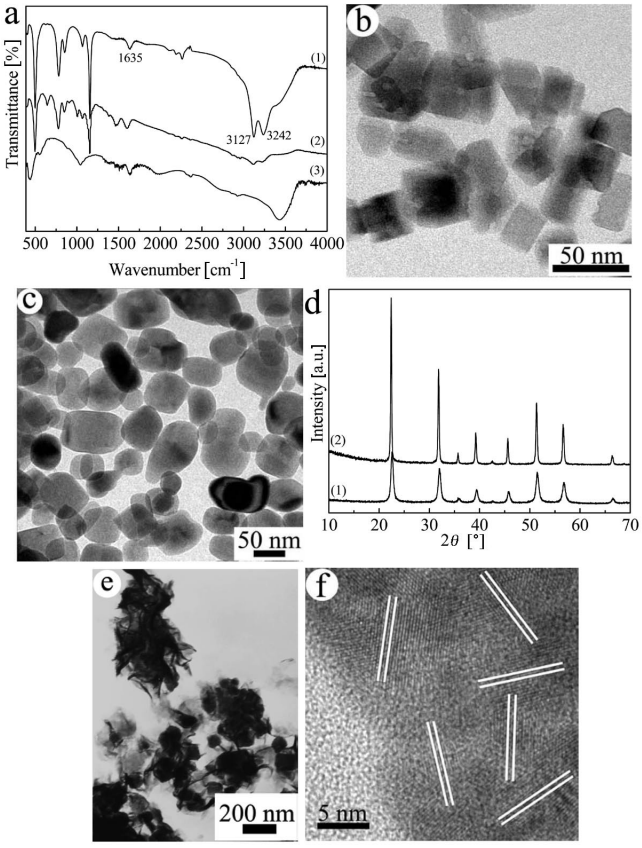

Figure 3. (a) IR spectra of samples prepared under different conditions: (1) V_{En} = 5 mL, (2) V_{En} = 0.1 mL, and (3) $V_{n\text{-butylamine}}$ = 5 mL. TEM images of samples obtained with different volume of En: (b) V_{En} = 0.5 mL and (c) V_{En} = 0.1 mL. (d) Curve 1 and 2 are XRD patterns of samples prepared at 210 °C after 16 and 1 h, respectively. (e) TEM images of samples obtained in alkaline media of *n*-butylamine.(f) HRTEM image of samples obtained after 1 h with V_{En} = 5 mL.

To access the interaction between the En molecules and $In(OH)_3$, we use FTIR spectroscopy to study the samples obtained at 210 °C for 16 h, as shown in curve (1) of Figure 3a. The FTIR spectrum clearly displays the ν(NH) vibration peaks of En at 3127 and 3242 cm^{-1} and the δ(NH) vibration peak at 1635 cm^{-1}. Both the ν(NH) and δ(NH) vibration peaks are shifted to higher frequency than the free En vibration due to the formation of hydrogen bonding.[39,40] This result confirms that the En molecules remain attached to the surfaces of the nanocubes in the separated sample. Through further exploration of the role of En in the formation process of aggregated nanocubes, it was also discovered that the morphologies of the $In(OH)_3$ nanostructures are sensitive to the amount of En. Although a slight increase or decrease in the amount of En did not seriously affect the formation of $In(OH)_3$ structures, a small amount of En ($V_{En} < 0.5$ mL) was not favorable for the formation of regular $In(OH)_3$ nanocubes (Figure 3b). When the amount of En was further decreased to 0.1 mL, the irregular $In(OH)_3$ nanoparticles did not assemble together (Figure 3c). We attribute this to a lack of En adsorbing onto the surface of $In(OH)_3$, which is suggested in the FTIR spectrum [Figure 3a, curve (2)]. In this figure, the ν(NH) vibration peaks of En and the δ(NH) vibration peak are very weak and do not obviously shift to higher frequency relative to those of free En. If another amine, such as *n*-butylamine, is substituted for En, no corresponding structures with self-assembled nanocubes were obtained in the final products (Figure 3e). As shown in curve (3) of Figure 3a, the FTIR spectrum of the sample does not display the characteristic peaks of the $-NH_2$ group, which reveals that *n*-butylamine did not adsorb to the surface of the final products. These results indicate that the En molecules are favorable for the oriented aggregation of the products as a result of the lack of surface-anchored organic molecules.

To better understand the mechanism for the self-assembly of the nanocubes, we collected a reaction intermediate product at an early reaction stage (reaction time is 1 h) for investigation. Curve (1) of Figure 3d shows the XRD pattern of the products, whose reflection peaks can be indexed to $In(OH)_3$. For better compassion, the XRD pattern of the final products is shown in curve (2) of Figure 3d. When the reaction time was extended, an increase in the crystallite size was obvious from the decrease in the peak width of curve (2) relative to curve (1). A typical HRTEM image (Figure 3f) reveals that facetted crystalline surfaces (indicated with the white lines) are already present and the orientation of the $In(OH)_3$ primary nanocrystals are random with various lattice directions.

Here, an organic-molecule-assisted self-assembly mechanism is proposed. In the initial reaction, the $In(OH)_3$ primary particles are formed. Upon extended heating, the particles further aggregate into nanocubes stabilized by En molecules that adsorb on the surface of the nanocubes in solution. Crystal growth of the stabilized nanocubes does not occur any further,[35] and self-assembly of En-coated nanocubes is strongly driven by interactions (such as van der Waals attraction) between the En molecules on adjacent nanocubes, but hindered by Brownian motion of $In(OH)_3$ nanocubes that are not favorable for self-assembly. Under the balance of van der Waals attraction and Brownian motion, $In(OH)_3$ nanocubes aggregated in an oriented manner to exhibit the features of single crystals, including crystallographic fusion between certain high-surface-energy faces. In this process, the nanocubes can find a low-energy configuration interface by rotation to give coherent lattice structures at the interfaces, because the formation of larger crystals can greatly reduce the interfacial energy of small nanocrystals.

Fabrication of Nanocube-Built $In(OH)_3$ Hollow and Solid Spherical Structures by Tuning the Reaction Temperature

Through systematic studies of varying growth parameters and detailed structures, it was also discovered that temperature plays an important role in controlling the self-assembly of $In(OH)_3$ nanocubes. The TEM images of a sample obtained at 180 °C, as shown in Figure 4, indicate

these nanocubes organize into quasisphere morphologies with diameters of 150–200 nm. It is clear that (Figure 4b) the cubes aggregate along circle chains, which further stack highly dimensional nanostructures by face-to-face alignment. The configuration adopted by the nanocubes at this temperature tends to be well ordered in comparison with the configuration of a sample obtained at 210 °C.

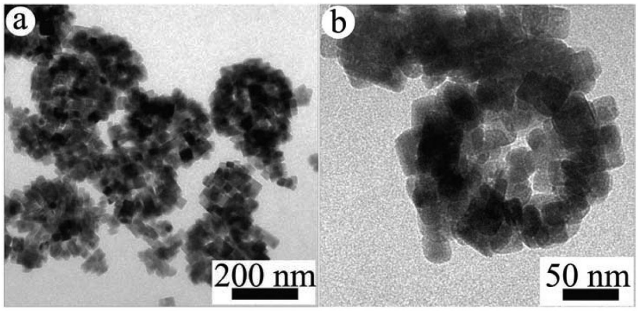

Figure 4. TEM image of $In(OH)_3$ quasispherical nanostructures at 180 °C: (a) low-magnification and (b) high-magnification images.

A decrease in the reaction temperature to 160 °C resulted in the formation of hollow spheres. The overall morphology of the product was obtained by field emission scanning electron microscopy (FE-SEM) and TEM. As shown in Figure 5a, the FE-SEM overview reveals that all samples are uniform spherical nanostructures with diameters of 400–500 nm. Some broken spheres present in the panoramic FE-SEM image, which suggests a hollow nature of the sample. A magnified FE-SEM image (Figure 5a, inset) of an open sphere further reveals that the products are hollow structures composed of nanocubes. Figure 5b shows a typical TEM image of the products, which clearly indicates that the $In(OH)_3$ sample consists of spherical nanostructures. The strong contrast between the dark edge and the pale center is further evidence for its hollow nature, and the thickness of a shell of the spheres is about 100 nm. Close analysis of the product (Figure 5b, inset) indicates that the as-prepared hollow spherical nanostructures are assembled by nanocubes with sizes around 50 nm.

When the reaction temperature was decreased to 140 °C, solid spheres rather than hollow spheres were obtained. Figures 5c and d show a panoramic FE-SEM and TEM image of the sample obtained at 140 °C, respectively. Figure 5c indicates that the sample consists of uniform spheres with diameters in the range of 1.5–2 μm. Open spheres cannot be found in the FE-SEM image, which suggests that the as-prepared products are solid spheres. Also, there are no lighter central parts corresponding to the void spaces in the TEM image of a sphere (Figure 5d), which reveals the solid spherical structure of the sample. Careful observation (Figure 5d and Figure 5c, inset) indicates that the surface of the solid spheres is composed of cubes with sizes larger than 100 nm.

Obviously, with decreasing temperatures, the morphology of $In(OH)_3$ changes from short-range, oriented, aggregated nanocubes to hollow and solid spheres composed of cubes. This suggests that relatively higher temperatures

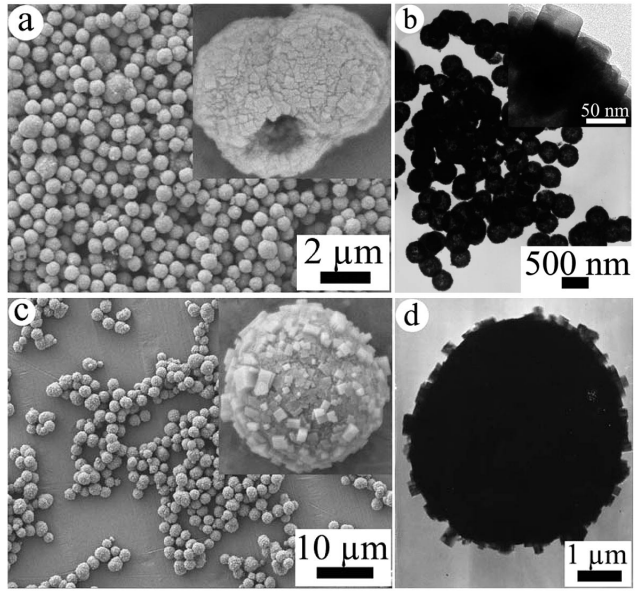

Figure 5. (a) A panoramic FE-SEM image and (b) a low-magnification TEM image of the obtained $In(OH)_3$ hollow spheres at 160 °C [the inset of (a) is an SEM image of the opened structure of a dual hollow sphere and that of (b) is a magnified TEM image taken from a hollow sphere edge]. (c) Panoramic FE-SEM and (d) TEM images of the obtained $In(OH)_3$ solid spheres at 140 °C [the inset of (c) is a magnified SEM image of a solid sphere].

are not favorable for the oriented aggregation of many nanocubes, because swift Brownian motion of the $In(OH)_3$ nonocrystals influences the long-range self-assembly. On the contrary, Brownian motion of $In(OH)_3$ nanocubes at low temperature is weaker than that at high temperature, whereas {100} crystal planes of *bcc* $In(OH)_3$ had equivalent aggregation potentials. Hence, van der Waals attractions among En molecules adsorbed to the surface of $In(OH)_3$ is much stronger than Brownian motion of $In(OH)_3$, which drives the self-assembly of the $In(OH)_3$ nanocubes to form solid spherical structures. Moreover, these nanocubes do not assemble into anisotropic structures but form spherical structures due to the {100} crystal planes of *bcc* $In(OH)_3$ having equivalent aggregation potentials.[15] The exact role of En molecules in this process is not clear and it needs to be investigated further.

Formation of C-In_2O_3 with Different Morphologies

C-In_2O_3 was prepared by annealing $In(OH)_3$ at 400 °C for 10 min under ambient pressure. The conversion process of the as-obtained $In(OH)_3$ sample during calcination in air was studied by thermogravimetry and differential thermal analysis (TG/DTA; Figure 6a). The TG curve of $In(OH)_3$ suggests that weight loss mainly occurs in the temperature range from 240 to 300 °C, and the weight loss of this step is about 15%. The DTA curve shows an endothermic reaction during this temperature range, which is ascribed to chemical dehydration of $In(OH)_3$ [2 $In(OH)_3 \rightarrow In_2O_3 + 3\ H_2O$]. These results of thermal analysis indicate that InOOH is

not formed during the dehydration process of $In(OH)_3$, and $In(OH)_3$ is directly convert into C-In_2O_3 in our experiment. Additionally, the weight loss between 120 and 240 °C can be attributed to the desorption of En from the surface of $In(OH)_3$, which suggests that En can be adsorbed on the surface of $In(OH)_3$ nanocrystals and is also consistent with the result of the IR spectrum.

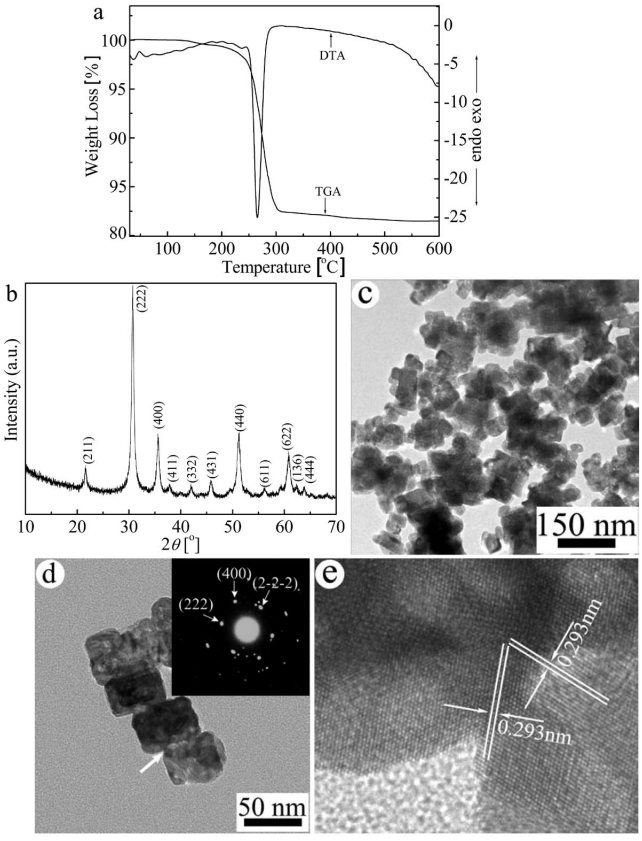

Figure 6. (a) TG and DTA curves of the obtained $In(OH)_3$ nanocubes at 210 °C. (b) XRD pattern of C-In_2O_3 nanocubes. TEM images of C-In_2O_3 samples: (c) at low-magnification and (d) typical aggregation of nanocubes (the inset is its corresponding SAED pattern). (e) HRTEM image obtained from the areas marked with a white arrow as shown in (d).

Figure 6b shows the XRD pattern of the product obtained by annealing $In(OH)_3$ precursors at 400 °C. All reflection peaks can be indexed as the cubic phase In_2O_3 (JCPDS No. 76–0152). No other impurities, such as In-OOH or H-In_2O_3, were detected, which is indicative of a sample with high purity. Figures 6c and d show the TEM images of C-In_2O_3 with irregular cube-like nanostructures, which indicates that In_2O_3 inherits the morphology of its precursors. However, its size slightly shrinks, because dehydration of $In(OH)_3$ during the calcination process causes high density.[30] Simultaneously, agglomeration of the nanoparticles is more serious in comparison with that of In-$(OH)_3$. These aggregated nanocubes are structurally uniform monocrystalline, which can be corroborated by the SAED pattern (Figure 6d, inset) and the HRTEM image (Figure 6e). The diffraction spots can be indexed to (222), $(2\bar{2}\bar{2})$, and (400) of cubic phase In_2O_3, which indicates that the HRTEM image was recorded with the electron beam along the $[01\bar{1}]$ zone axis. From the HRTEM image of the coalescent area marked with a white arrow in Figure 6d, both lattice fringes are ca. 0.293 nm, which is consistent with the (222) and $(2\bar{2}\bar{2})$ crystal planes of C-In_2O_3, respectively. These results reveal that the uniform alignment of space fringes between nanocubes is still existent.

FE-SEM and TEM analyses (Figure 7) were performed to examine the morphologies of other In_2O_3 samples obtained by calcinating different precursors (prepared at 160 and 140 °C, respectively). The panoramic observation (Figure 7a) reveals that the as-obtained In_2O_3 sample inherits the morphology of the $In(OH)_3$ precursor obtained at 160 °C, and it is a well-shaped sphere-like structure with a diameter of ca. 500 nm. A magnified SEM image (Figure 7a, inset) of an open sphere further reveals that the hollow sphere structures do not collapse during the calcination process and also confirms that the hollow spheres are assembled by distorted cubes. The contrast in the TEM image (Figure 7b) shows that the as-obtained In_2O_3 sample is a hollow spherical nanostructure. Similarly, Figure 7c represents the FE-SEM images of solid In_2O_3 spherical structures with a diameter of 1.5–2 μm. The solid trait of the as-obtained In_2O_3 sample is also testified by the TEM image in Figure 7d, where there is no strong contrast between the center and the edge of the sphere. Through careful observation (Figure 7c, inset), we find that the subunits in the spherical structures are shrinking nanocubes. This result indicates that the original shape is kept in the phase transformation from $In(OH)_3$ into In_2O_3 after calcination in air, and the well-shaped spherical structures of In_2O_3 are composed of distorted cubes as a result of the dehydration of $In(OH)_3$.

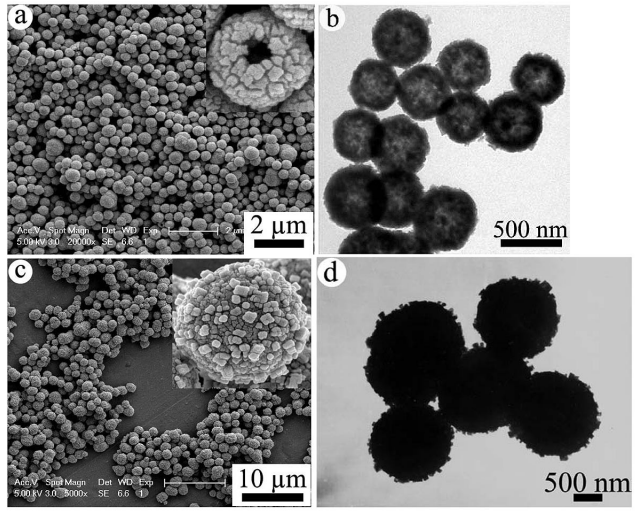

Figure 7. (a) Panoramic FE-SEM and (b) low-magnification TEM images of In_2O_3 hollow spheres [the inset of (a) is an SEM image of an opened hollow sphere]. (c) Panoramic FE-SEM and (d) TEM images of In_2O_3 solid spheres [the inset of (c) is a magnified SEM image of a solid sphere].

Optical Properties

The photoluminescent (PL) properties of C-In_2O_3 samples with different morphologies were investigated. These samples show a PL emission in the blue spectral region under UV light irradiation (λ_{ex} = 260 nm), and their PL properties are similar. Figure 8 shows the PL emission spectrum for the irregular In_2O_3 nanocubes, which consists of an emission peak located at 437 nm. In previous investigations, the PL spectra of In_2O_3 with peaks at different wavelengths were reported; the emission discrepancies were mainly attributed to the presence of oxygen vacancies (VOs),[34,41–47] except lower wavelengths (326–332 nm) close to the peaks of the bandgap were observed.[48,49] Here, the In_2O_3 samples were prepared from $In(OH)_3$ precursors after annealing at 400 °C, and the VOs can be generated in this process because the oxygen-induced lower energy level is a nonstable state and the probability of electron jump is small. Hence, under UV irradiation, electrons are excited from the valence band (VB) to the conduction band (CB) instead of to the oxygen-induced lower energy level. Electrons move freely in the CB and finally relax to the oxygen vacancies. The recombination of an electron with a hole yields the blue emission. The blue emission of In_2O_3 can be illustrated in Scheme 1, and we think that the emission peaks are related to the energy levels produced by VOs.

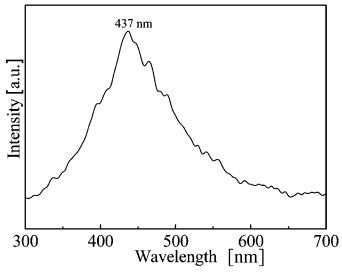

Figure 8. PL emission spectrum of In_2O_3 irregular nanocubes.

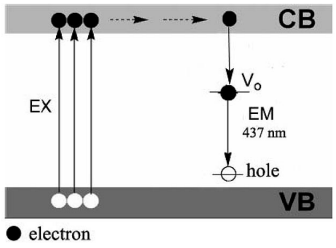

Scheme 1. Schematic illustration of excitation and emission process of In_2O_3.

Conclusions

$In(OH)_3$ and C-In_2O_3 nano/microstructures with different morphologies were successfully prepared by a simple hydrothermal method with the assistance of En conditions. The shape and size of $In(OH)_3$ and In_2O_3 can be modulated by tuning the reaction temperature. Such a synthetic route is interesting in investigating particle-oriented aggregation with building blocks, and it is expected that this technique could be used to prepare other 3D architectures.

Experimental Section

Materials: Indium trichloride tetrahydrate ($InCl_3 \cdot 4H_2O$) and ethylenediamine (En) were analytical grade reagents and purchased from Shanghai Chemical Company. All reagents were used as received without further purification.

Synthesis of $In(OH)_3$ Nanocubes, Hollow Spheres, and Solid Spheres: The $In(OH)_3$ nanocubes were prepared according to a modified method similar to that reported in the literature.[50] Typically, after $InCl_3 \cdot 4H_2O$ (0.5 mmol) was mixed with deionized water (40 mL), En (5 mL) was added into this mixture at room temperature. The solution was stirred for 5 min and then was transferred into a 50-mL Teflon-lined autoclave. The autoclave was sealed and maintained at 210 °C for 16 h in a digital temperature-controlled oven. After the autoclave was cooled to room temperature naturally, the products were separated by centrifugation, washing with distilled water and ethanol several times, and drying in a vacuum at 50 °C for 4 h. The hollow and solid spheres were prepared at temperatures of 160 and 140 °C whilst keeping all other parameters unchanged.

Synthesis of C-In_2O_3 Nanocubes, Hollow Spheres, and Solid Spheres: The presynthesized white samples (obtained at 210, 160, and 140 °C) were loaded into a quartz boat and annealed in a tube furnace at 400 °C for 10 min under ambient pressure and then cooled down to room temperature naturally. The heat rate for the tube furnace was 10 °C min^{-1} until the furnace temperature reached 400 °C. The final pale yellow C-In_2O_3 products were collected for subsequent characterization.

Characterization: The crystal phase of the as-prepared products was characterized by using a Philips X′Pert SUPER powder X-ray diffractometer with Cu-K_α radiation (λ = 1.5418 Å). The morphologies and structural analyses of the samples were carried out by TEM, SAED, and HRTEM (JEOL 2010 high resolution transmission electron microscope, with an accelerating voltage of 200 kV), and FESEM (JSM-6700F field emission scanning electron microanalyzer, with an accelerating voltage of 10 kV). Reflection infrared analysis was performed with a PerkinElmer FTIR spectrophotometer at room temperature. Thermogravimetry and differential thermal analysis measurements were performed with a Shimadzu TA-50WS analyzer in N_2 gas in the temperature range from room temperature to 600 °C. the photoluminescence spectrum was obtained with a Hitachi 850 fluorescence spectrophotometer.

Acknowledgments

Financial support from the National Nature Science Research Foundation of China is gratefully acknowledged.

[1] E. Baumeister, S. Klaeger, *Adv. Eng. Mater.* **2003**, *5*, 673–677.
[2] J. Huang, Y. Xie, B. Liu, Y. Qian, S. Zhang, *Adv. Mater.* **2000**, *12*, 808–811.
[3] Y. Zhu, J. Shi, W. Shen, X. Dong, J. Feng, M. Ruan, Y. Li, *Angew. Chem. Int. Ed.* **2005**, *44*, 5083–5087.
[4] X. Gao, J. Zhang, L. Zhang, *Adv. Mater.* **2002**, *14*, 290–293.
[5] R. L. Penn, J. F. Banfield, *Science* **1998**, *281*, 969–971.
[6] J. F. Banfield, S. A. Welch, H. Zhang, T. T. Ebert, R. L. Penn, *Science* **2000**, *289*, 751–754.

[7] A. P. Alivisatos, *Science* **2000**, *289*, 736–737.
[8] C. Pacholski, A. Kornowski, H. Weller, *Angew. Chem. Int. Ed.* **2002**, *41*, 1188–1191.
[9] B. Nikoobakht, Z. L. Wang, M. A. Elsayed, *J. Phys. Chem. B* **2000**, *104*, 8635–8640.
[10] G. M. Whitesides, B. Grzybowski, *Science* **2002**, *295*, 2418–2421.
[11] Z. Tang, N. A. Kotov, M. Gierisg, *Science* **2002**, *297*, 237–240.
[12] Z. Zhang, M. Han, *Chem. Phys. Lett.* **2003**, *374*, 91–94.
[13] R. L. Penn, G. Oskam, T. J. Strathmann, P. C. Searson, A. T. Stone, D. R. Veblen, *J. Phys. Chem. B* **2001**, *105*, 2177–2182.
[14] T. He, D. Chen, X. Jiao, *Chem. Mater.* **2004**, *16*, 737–743.
[15] Z. Zhang, H. Sun, X. Shao, D. Li, H. Yu, M. Han, *Adv. Mater.* **2005**, *17*, 42–47.
[16] D. Yu, X. Sun, J. Zou, Z. Wang, F. Wang, K. Tang, *J. Phys. Chem. B* **2006**, *110*, 21667–21671.
[17] J. Y. Gong, S. H. Yu, H. S. Qian, L. B. Luo, X. M. Liu, *Chem. Mater.* **2006**, *18*, 2012–2015.
[18] Y. Zhu, W. Zhao, H. Chen, J. Shi, *J. Phys. Chem. C* **2007**, *111*, 5281–5285.
[19] N. Bowden, A. Terfort, J. Carbeck, G. M. Whitesides, *Science* **1997**, *276*, 233–235.
[20] K. P. Velikov, C. G. Christova, R. P. A. Dullens, A. Blaaderen, *Science* **2002**, *296*, 106–109.
[21] D. H. Gracias, J. Tien, T. L. Breen, C. Hsu, G. M. Whitesides, *Science* **2000**, *289*, 1170–1172.
[22] J. C. Love, A. R. Urbach, M. G. Prentiss, G. M. Whitesides, *J. Am. Chem. Soc.* **2003**, *125*, 12696–12697.
[23] C. R. Mayer, S. Neveu, V. Cabuil, *Adv. Mater.* **2002**, *14*, 595–597.
[24] S. Park, J. H. Lim, S. W. Chung, C. A. Mirkin, *Science* **2004**, *303*, 348–351.
[25] I. Hamberg, C. G. Granqvist, *J. Appl. Phys.* **1986**, *60*, 123–160.
[26] E. Gagaoudakis, M. Bender, E. Douloufakis, N. Kataarakis, N. Natsakou, V. Cimalla, G. Kiriakids, *Sens. Actuator, B* **2001**, *80*, 155–161.
[27] W. Y. Chung, G. Sakai, K. Shimanoe, N. Miura, D. D. Lee, N. Yamazoe, *Sens. Actuator, B* **1998**, *46*, 139–145.
[28] M. Liess, *Thin Solid Films* **2002**, *410*, 183–187.
[29] J. Tamaki, C. Naruo, Y. Yamanoto, M. Matsuoka, *Sens. Actuator, B* **2002**, *83*, 190–194.
[30] B. Li, Y. Xie, M. Jing, G. Rong, Y. Tang, G. Zhang, *Langmuir* **2006**, *22*, 9380–9385.
[31] Q. Tang, W. Zhou, W. Zhang, S. Ou, K. Jiang, W. Yu, Y. Qian, *Cryst. Growth Des.* **2005**, *5*, 147–150.
[32] D. Yu, S. H. Yu, S. Zhang, J. Zuo, D. Wang, Y. Qian, *Adv. Funct. Mater.* **2003**, *13*, 497–501.
[33] C. Chen, D. Chen, X. Jiao, C. Wang, *Chem. Commun.* **2006**, *44*, 4632–4634.
[34] J. Yang, C. Liu, Z. Wang, J. Lin, *Inorg. Chem.* **2006**, *45*, 8973–8979.
[35] J. Huang, L. Gao, *J. Am. Ceram. Soc.* **2006**, *89*, 724–727.
[36] Z. Zhuang, Q. Peng, J. Liu, X. Wang, Y. Li, *Inorg. Chem.* **2007**, *46*, 5179–5187.
[37] H. Cölfen, S. Mann, *Angew. Chem. Int. Ed.* **2003**, *42*, 2350–2365.
[38] C. Li, X. Lu, Y. Liang, *Langmuir* **2002**, *18*, 575–580.
[39] S. Gorai, D. Ganguli, S. Chaudhuri, *Cryst. Growth Des.* **2005**, *5*, 875–877.
[40] J. Yang, J. H. Zeng, S. H. Yu, L. Yang, G. E. Zhou, Y. T. Qian, *Chem. Mater.* **2000**, *12*, 3259–3263.
[41] H. Zhou, W. Cai, L. Zhang, *Appl. Phys. Lett.* **1999**, *75*, 495–497.
[42] C. Ling, G. Meng, Y. Lei, F. Phillipp, L. Zhang, *Adv. Mater.* **2001**, *13*, 1330–1333.
[43] M. J. Zheng, L. D. Zhang, G. H. Li, X. Y. Zhang, X. F. Wang, *Appl. Phys. Lett.* **2001**, *79*, 839–841.
[44] X. C. Wu, J. M. Hong, Z. J. Han, Y. R. Tao, *Chem. Phys. Lett.* **2003**, *373*, 28–32.
[45] P. Guha, S. Kar, S. Chaudhuri, *Appl. Phys. Lett.* **2004**, *85*, 3851–3853.
[46] Q. Liu, W. Lu, A. Ma, J. Tang, J. Lin, J. Fang, *J. Am. Chem. Soc.* **2005**, *127*, 5276–5277.
[47] Y. Lei, W. K. Chim, *J. Am. Chem. Soc.* **2005**, *127*, 1487–1492.
[48] W. S. Seo, H. H. Jo, K. Lee, J. T. Park, *Adv. Mater.* **2003**, *15*, 795–797.
[49] A. Murali, A. Barve, V. J. Leppert, S. H. Risbud, *Nano Lett.* **2001**, *1*, 287–289.
[50] J. Huang, L. Gao, *Cryst. Growth Des.* **2006**, *6*, 1528–1532.

Received: September 7, 2007
Published Online: January 31, 2008

